Nucl. Instr. Meth. B 194 (2002) 177–186

Ion Beam Analysis of Rough Thin Films

M. Mayer

Max-Planck-Institut für Plasmaphysik, EURATOM Association, Boltzmannstr. 2, D-85748 Garching, Germany

Abstract

The influence of surface roughness on RBS spectra has been studied experimentally and by computer simulation with the SIMNRA code. Rough thin films are described by a distribution of film thicknesses, while rough substrates are approximated by a distribution of local inclination angles. Correlation effects of surface roughness are neglected. Rough film effects can be calculated for RBS including non-Rutherford scattering, NRA and ERDA. The results of simulation calculations show good agreement with experimental data. For thin films of high Z elements on rough substrates additionally plural scattering plays an important role.

1 Introduction

Rutherford backscattering spectroscopy (RBS), nuclear reaction analysis (NRA) and elastic recoil detection analysis (ERDA) with incident MeV ions are powerful methods for the quantitative analysis of thin films and depth profiling of the near-surface layers of solids [1]. However, the quantitative application of these methods is restricted to laterally homogeneous and smooth films. Several computer codes for the evaluation of RBS, NRA and ERDA spectra assuming a multi-layered, smooth sample structure are available, such as RUMP [2,3] or SIMNRA [4,5].

The experimentalist is often confronted with rough surfaces. The effects of rough surfaces of *thick* targets on RBS were investigated in some detail by Edge and Bill [6], Knudson [7], Bird *et al.* [8], and Hobbs *et al.* [9]. Wüest and Bochsler [10] and Yesil *et al.* [11,12] attacked the problem by means of a Monte-Carlo computer simulation, taking into account correlation effects of the surface roughness and multiple surface crossings of the incident and emerging ions. It turned out that effects of rough surfaces of *thick* targets occur only for grazing angles of the incident or emerging ions. This is for example the case in ERDA applications on thick, rough targets,

as was shown by Yesil *et al.* [11,12] and Kitamura *et al.* [13]. Hydrogen depth profiling on rough surfaces by ERDA was studied experimentally by Behrisch *et al.* [14].

Astonishingly, the effects of rough *thin films* were studied much more scarcely. For RBS, rough films on a smooth substrate (Fig. 1a) were investigated by Shorin and Sosnin [15] and Metzner *et al.* [16,17]. Shorin and Sosnin [15] used a Monte-Carlo computer simulation. The Monte-Carlo approach suffers from long computing times of the order of hours [12], rendering these codes impractical for evaluation of experimental spectra. Moreover, the Shorin/Sosnin code treats only RBS with Rutherford cross-sections, neglecting non-Rutherford scattering, NRA and ERDA. The theoretical approach of Metzner *et al.* [16,17] allows to extract the thickness distribution of rough films from a measured spectrum. However, this approach is only valid for RBS with Rutherford cross sections, a scattering angle of exactly 180° and constant stopping power, thus severely limiting the practical applicability of this work. The computer code RUMP [2,3] allows to blur the interface between two layers by roughening the top layer. However, this is intended only for small roughness amplitudes, the roughness distribution function is not documented, and comparisons to experimental data are not available.

Moreover, all work done so far treats only the case of a rough film on a smooth substrate. But in practice also the case of a film deposited on a rough substrate (Fig. 1b) is sometimes encountered. Surface roughness has been added to the well known simulation code SIMNRA [4,5], version 4.70 and higher. The code can treat one or more rough layers on a rough substrate and rough foils in front of the detector for RBS (including non-Rutherford scattering), ERDA and NRA. This paper describes the used algorithms and compares results of code calculations with experimental data. The limitations of the used approximations are discussed.

2 The SIMNRA code

The SIMNRA code has been described in detail elsewhere [4,5]. It is a Microsoft Windows 95/98/NT/2000/XP program with fully graphical user interface for the simulation of non-Rutherford backscattering, nuclear reaction analysis and elastic recoil detection analysis with MeV ions. About 300 different non-Rutherford and nuclear reactions cross-sections are included. SIMNRA can calculate any ion-target combination including incident heavy ions and any geometry including transmission geometry. Arbitrary multi-layered foils in front of the detector can be used. For electronic energy loss either the stopping power data by Andersen and Ziegler [18,19] or the more recent data by Ziegler, Biersack and Littmark [20] can be used. The electronic stopping power of heavy ions is derived from the stopping power of protons using Brandt-Kitagawa the-

ory [20,21] with the same algorithm as used in TRIM 97. Energy loss straggling includes the corrections by Chu to Bohr's straggling theory [22,23], propagation of straggling in thick layers, and geometrical straggling. Multiple *small angle* scattering results in an additional, nearly Gaussian shaped straggling contribution, which is calculated according to [24,25]. Multiple scattering with 2, 3, 4... scattering events with *large* deflection angles is called plural scattering. It results in a non-Gaussian shaped background contribution and can be calculated approximately in the dual scattering approximation by SIMNRA, where 2 scattering events with large deflection angles are taken into account [26]. The dual scattering approximation underestimates the plural scattering background somewhat due to the disregard of trajectories with 3, 4... deflections [26]. Major drawback of the dual scattering approximation is the large increase in computing time by a factor of about 200.

3 Experimental

RBS measurements were performed at the 3 MV Tandem accelerator at the IPP Garching. Backscattered particles were recorded with a PIPS detector at a scattering angle of 165°. Most measurements were performed in the RKS facility, with a detector solid angle of 1.14×10^{-3} sr and a beam spot size on the target of 1×1 mm^2. The detector resolution for 2 MeV ^{4}He ions was about 14 keV. The target current is measured with a Farraday-cup with an accuracy better than about 3%. W layers were analyzed in the BOMBARDINO experiment, which allows to handle large targets up to 300×200 mm^2. The beam spot had a diameter of 1.8 mm, and the detector solid angle was about 3×10^{-4} sr. The beam current measurement was not sufficiently reliable, therefore the spectra were normalized to the height of the W spectrum.

Line profiles of target surfaces were determined with a mechanical profiler (Tencor Alpha-Step 200) with a vertical resolution of 5 nm, a horizontal step width of 1 μm and a scan length of 2 mm in 40 s. The profiler tip was conical with an apex angle of about 60°.

4 Rough film on a smooth substrate

A rough film on a smooth substrate is shown schematically in Fig. 1a. The substrate can be considered to be smooth, if its roughness is much smaller than the mean thickness $\bar{d}$ of the film. The film thickness distribution is described by a distribution function $p(d)$, with the film thickness d measured perpendicular to the substrate, see Fig. 1a, and $d \geq 0$. In the literature, usually a Gaussian distribution centered at $\bar{d}$ with variance σ^2 and cut-off at zero is used for $p(d)$ [16,17]. However, a more natural choice of a distribution function with only positive values $d \geq 0$ is the Gamma distribution, which is

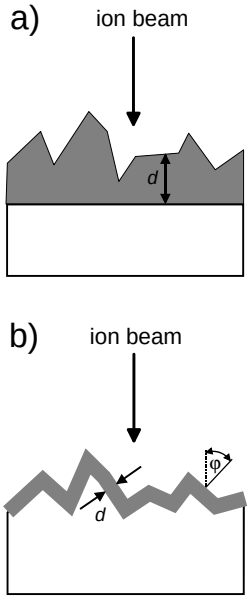

Fig. 1. Schematic representation of a rough film on a smooth substrate (a), and of a smooth film on a rough substrate (b). Grey: Film; white: Substrate.

also fully described by its mean value $\bar{d}$ and standard deviation σ. The Gamma distribution is defined by

$$p(d) = \frac{\beta^\alpha}{\Gamma(\alpha)} d^{\alpha-1} e^{-\beta d}, d > 0 \qquad (1)$$

with $\alpha = \bar{d}^2/\sigma^2$ and $\beta = \bar{d}/\sigma^2$. $\Gamma(\alpha)$ is the Gamma function. The Gamma distribution is shown in Fig. 2 for $\bar{d} = 1$ and different standard deviations σ. The corresponding Gaussian distributions centered at 1 and identical σ are shown for comparison. For small roughnesses with $\sigma \ll \bar{d}$, i.e. if the width of the distribution is small compared to its mean value, Gaussian and Gamma distributions are nearly identical, see the curves for $\sigma = 0.1$ in Fig. 2. With increasing σ the two distributions become more and more different (see the curves for $\sigma = 0.3$ and 0.7 in Fig. 2). For $\sigma = \bar{d}$ the Gamma distribution decreases

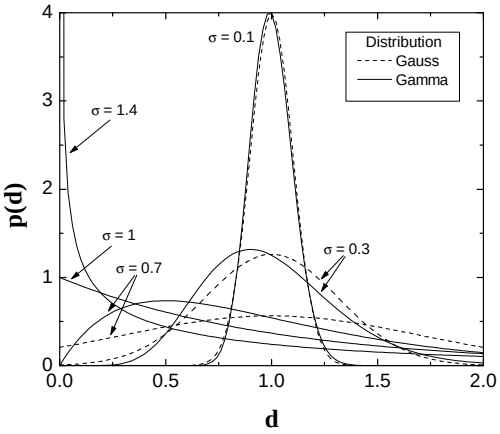

Fig. 2. Comparison of Gaussian distribution functions centered at 1 (dashed lines) and Gamma distribution functions (solid lines) with mean value $\bar{d} = 1$ and different standard deviations σ.

exponentially with $p(d) = e^{-d}$, and for $\sigma > \bar{d}$ an integrable singularity develops at $d = 0$.

A RBS, NRA or ERDA spectrum of a rough film is approximated by a superposition of N spectra with different layer thicknesses d_i. Typically about $N = 20$ sub-spectra are necessary to obtain a smooth superposition, though N has to be increased to about $N = 50$ for broad distributions with $\sigma \geq \bar{d}$. The weight w_i of each sub-spectrum is determined according to the thickness distribution function. For each sub-spectrum the layer is treated to be smooth with thickness d_i. Correlation effects, such as incidence through a hump and emergence through a valley or multiple surface crossings, are neglected. This is only correct for backscattering at a scattering angle of exactly 180° and for transmission geometries. However, for scattering angles in the range 150°–180° and non-grazing incidence and emergence angles, as are used in many RBS and

NRA setups, correlation effects still play only a minor role and can be neglected without severe loss of accuracy. But it should be kept in mind that the used approximation gets invalid for grazing incidence or exit angles, as is the case in ERDA - in these cases correlation effects may be dominant and can change the shape of the spectra considerably.

The effect of layer roughness on the shape of RBS spectra is shown in Fig. 3 for incident ^{4}He ions backscattered from a gold layer at a scattering angle of 165°. The spectra were calculated with the SIMNRA code, the film thickness distributions are described by the Gamma distributions shown in Fig. 2. If the thickness variation is much smaller than the mean film thickness ($\sigma/\bar{d} = 0.1$), only the low energy edge of the film is affected by the roughness and gets broader. With increasing roughness the broadening of the low energy edge increases, until at $\sigma/\bar{d} \approx 0.6$ the high energy edge begins to decrease. The energy $E_{1/2}$, at which the low energy edge has decreased to its half height, remains fairly constant until large roughness amplitudes of the order $\sigma/\bar{d} \approx 0.6$, i.e. until the high energy edge begins to decrease. For sufficiently thick films, i.e. if the film is completely resolved, this energy is therefore a rather robust measure of the mean film thickness even for large roughnesses, as long as the high energy edge is not affected.

The energy spectrum of 1.5 MeV ^{4}He backscattered from a rough Ni-film deposited on polycrystalline carbon is shown in Fig. 4. The experimental

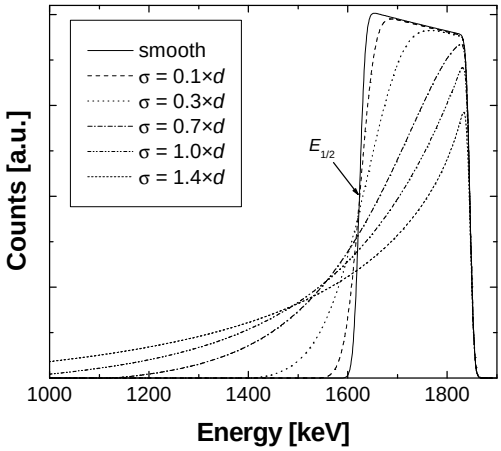

Fig. 3. Calculated energy spectra for 2 MeV ^{4}He backscattered from a smooth and rough gold layers with mean thickness $\bar{d} = 1 \times 10^{18}$ Au-atoms/cm^2 and different roughnesses with standard deviation σ. The film thickness distributions are shown in Fig. 2. Incident angle $\alpha = 0°$, scattering angle 165°. $E_{1/2}$ marks the energy, at which the low energy edge has decreased to its half height.

data are not well reproduced by the simulated spectrum of a smooth Ni layer (dashed line). The measured spectrum is well reproduced in the simulation by a mean Ni layer thickness of 2.17×10^{18} Ni-atoms/cm^2 (238 nm) and a roughness with standard deviation $\sigma = 2.12 \times 10^{17}$ Ni-atoms/cm^2 (23 nm) (solid line). The remaining discrepancies between experimental data and simulation, especially the small background in channels 120–400, are mainly due to impurities and plural scattering in the Ni layer, which was not taken into account in the calculation.

The roughness of the Ni film was determined from line scans with a profiler. The roughness distribution, i.e. the deviation of the actual surface from the leveled one, was approxi-

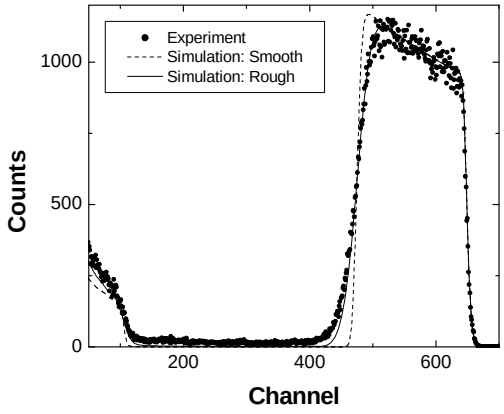

Fig. 4. 1.5 MeV ^{4}He backscattered at 165° from a rough Ni-film with a mean thickness of 2.17×10^{18} Ni-atoms/cm^2 on carbon substrate. Dots: Experimental data; Dashed line: Simulation assuming a smooth Ni layer; Solid line: Simulation assuming a rough Ni layer with roughness $\sigma = 2.12 \times 10^{17}$ Ni-atoms/cm^2.

mately Gaussian: For small values of $\sigma/\bar{d}$ a Gaussian and a Gamma distribution cannot be distinguished, see Fig. 2. The carbon substrate was already rough with a standard deviation $\sigma_{\mathrm{C}} = 18.2$ nm. The roughness of the Ni film on the substrate was $\sigma_{\mathrm{C+Ni}} = 26.5$ nm. This roughness is made up by the roughness of the carbon substrate plus the roughness of the Ni film σ_{Ni}. By assuming the two roughnesses to be independent, i.e. $\sigma^2_{\mathrm{C+Ni}} = \sigma^2_{\mathrm{C}} + \sigma^2_{\mathrm{Ni}}$, the roughness of the Ni film alone is about 19.3 nm. Keeping in mind that this value may have a large error, because it is derived as the difference of two numbers, this is in very good agreement with the result from He backscattering of 23 nm (Fig. 4).

The energy spectrum of 2.0 MeV ^{4}He backscattered from a rough oxidised aluminum film on polycrystalline carbon substrate is shown in Fig. 5. The carbon substrate was well polished and had a mean roughness < 25 nm [27]. The film was exposed for about 8 months as erosion monitor at the vessel wall of the nuclear fusion tokamak experiment JET [28,27], the wall temperature was about 300°C. The initial Al layer thickness was 3.16×10^{18} atoms/cm^2 (525 nm), but decreased due to sputtering by bombardment with energetic hydrogen atoms from the nuclear fusion plasma to 7.5×10^{17} Al-atoms/cm^2. At the same time the Al film was oxidised and some nickel, which was initially eroded at an erosion dominated area of the JET vessel wall [1], was redeposited on the Al film and incorporated. The observed spectrum with the tails at the low energy sides of the O, Al and Ni peaks cannot be reproduced by assuming a smooth layer. But it is fairly well reproduced by a rough layer with a mean film thickness of 1.11×10^{18} atoms/cm^2, roughness $\sigma = 1.06 \times 10^{18}$ atoms/cm^2, and composition 68% Al, 30% O, 2% Ni (solid line in Fig. 5). The shape of the film thickness distribution is close to the curve with $\sigma = 1$ in Fig. 2. This example shows clearly that non-Gaussian distributions of layer thicknesses are observed in practice and can be described by a Gamma distribution.

[1] The JET vessel walls consist of Inconel, a stainless steel with high nickel content.

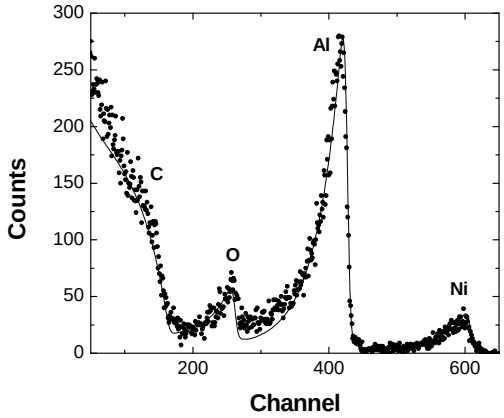

Fig. 5. 2 MeV ^{4}He backscattered at 165° from a rough oxidised aluminum film on carbon. The film was used as long term sample in the tokamak JET and was strongly eroded by plasma impact. Additionally some Ni was deposited from the plasma. Dots: Experimental data; Solid line: Simulation with a mean film thickness of 1.11×10^{18} atoms/cm^2 and roughness $\sigma = 1.06 \times 10^{18}$ atoms/cm^2. Film composition 68% Al, 30% O, 2% Ni.

5 Smooth film on a rough substrate

A film with homogeneous thickness d on a rough substrate is shown schematically in Fig. 1b. The substrate is considered to be rough, if its roughness amplitude is much larger than the thickness d of the film. We assume a rough substrate to consist of inclined line segments with local inclination angle φ, and the film thickness d is measured parallel to the local surface normal. Such a rough surface is described by a distribution of local tilt angles $p(\varphi)$. The concept of a local tilt angle was already used by Küstner *et al.* for the calculation of the sputtering yield of rough surfaces by ion bombardment in the energy range 100 eV to several keV [29]. In Küstner's work the rough surface was treated as a fully 3-dimensional object, which was necessary due to the 3-dimensional nature of the collision cascades created by keV ions. In MeV ion beam analysis the trajectories of the incident and emerging ions can be approximated with good accuracy by straight lines, and we have to consider only the intersection of the plane, which is spanned by the trajectories of the incident and emerging ions, and the target surface, see Fig. 6: The intersection is only a 2-dimensional line profile as the one shown in Fig. 1b.

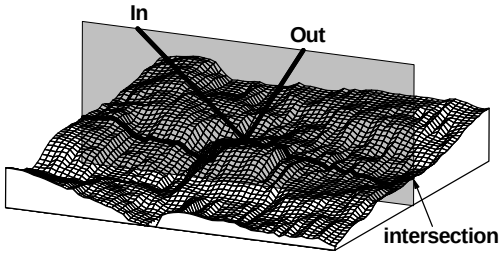

Fig. 6. Schematic representation of a rough surface. In: Direction of the incident beam; Out: Direction of the outgoing beam; Light gray: Plane spanned by the incident and outgoing beams; Intersection: Intersection of the plane with the rough surface.

The tilt angle distribution is given by $p(\varphi)$. This distribution describes the frequency of occurence of a line segment inclined by φ. A rough surface without preferential orientation has a mean tilt angle

$$\bar{\varphi} = \int_{-90^\circ}^{90^\circ} \varphi \, p(\varphi) \, d\varphi = 0^\circ. \qquad (2)$$

The probability distribution $\tilde{p}(\varphi)$ of hitting a surface tilted by φ by an

incident ion is given by

$$\tilde{p}(\varphi) = p(\varphi)\cos(\alpha - \varphi), \qquad (3)$$

with the incident angle α of the ion. α is measured towards the surface normal of a non-inclined surface. The factor $\cos(\alpha - \varphi)$ is due to the projection of the line segment into the plane perpendicular to the incident ion trajectory: It is more likely to hit a segment which is perpendicular to the incident trajectory than an inclined segment - and obviously it is impossible to hit a segment which is tilted parallel to the incident beam. It is important to note that a profiler or a scanning tunneling microscope (STM), which samples the surface at a constant step width parallel to the surface, measures the distribution $\tilde{p}(\varphi)$ rather than $p(\varphi)$: Large tilt angles are under-represented in the measurement, and tilt angles of 90° cannot be measured at all by a profiler or STM.

RBS, NRA and ERDA spectra of a smooth film on a rough substrate are approximated by a superposition of M spectra with different local incident and emerging angles $\tilde{\alpha} = |\alpha - \varphi|$ and $\tilde{\beta} = |\beta + \varphi|$. The weight of each sub-spectrum is determined according to the distribution function $\tilde{p}(\varphi)$. For each sub-spectrum the substrate is treated to be smooth, i.e. a spectrum for a smooth layer, but with incident angle $\tilde{\alpha}$ and emergence angle $\tilde{\beta}$ is calculated. Incident angles $\tilde{\alpha} > 90°$ are excluded: This represents a line segment which cannot be hit by the incident beam. As in the case of a rough film on a smooth substrate, surface correlation effects like shadowing of one line segment by another, and multiple surface crossings are neglected.

Which distribution should be used as tilt angle distribution $p(\varphi)$? We have investigated different rough surfaces with a profiler. As will be shown elsewhere [30], a Gaussian distribution of tilt angles usually underestimates strongly the wings of the distribution, while a Lorentz distribution yields a reasonable fit to the measured data. The correct measurement of large inclination angles $> \pm 45°$ with a profiler is an experimental problem due to the finite step width and the apex angle of the profiler tip, resulting in larger uncertainties especially in the wings of the distribution. Provided that the calculation model is correct, the application of Bayesian data analysis methods allows extraction of the tilt angle distribution from measured ion beam backscattering spectra more accurately [30].

In the following we describe the tilt angle distribution by a Lorentz distribution centered a 0°. The only free parameter of the distribution is the full width at half maximum (FWHM). If a given surface is correctly described by this model or not has to be checked in each case by measuring surface profiles.

Calculated backscattering spectra for ^{4}He ions at normal incidence backscattered from a gold layer with thickness 1×10^{18} atoms/cm^2 and a scattering angle of 165° are shown in Fig. 7 for a smooth and rough

substrates. Plural scattering was neglected. The rough substrates are described by a Lorentz distribution of tilt angles with different FWHM w. On a rough substrate the low energy edge gets a tail, which increases with increasing roughness. This tail extends to energies close to zero. With increasing roughness the Au peak gets broader, and the energy $E_{1/2}$, at which the low energy edge has decreased to its half height, is not a good measure of the film thickness: It depends on the roughness of the substrate. The high energy edge and the plateau (in the energy range 1650–1800 keV) are only slightly affected by substrate roughness and decrease only little at large roughnesses due to shadowing: The backscattered particles do not reach the detector any more, because the exit angle β points inside the layer. For $w = \infty$ the local tilt angles are equipartitioned, and the corresponding spectrum represents the case of maximum roughness.

A measured spectrum for 2.5 MeV protons backscattered from a tungsten layer on a rough carbon substrate is shown in Fig. 8. The non-Rutherford elastic scattering data from [31] were used for the C(p,p)C cross section. The substrate is a carbon fibre composite (CFC) material manufactured by Dunlop, which is used for high heat flux components in the tokamak experiment JET due to its high thermal conductivity. The surface was milled, but not polished, and the W layer was deposited from a pulsed cathodic arc discharge at DIARC Technology Inc. (Finland) at room temperature. The mean W

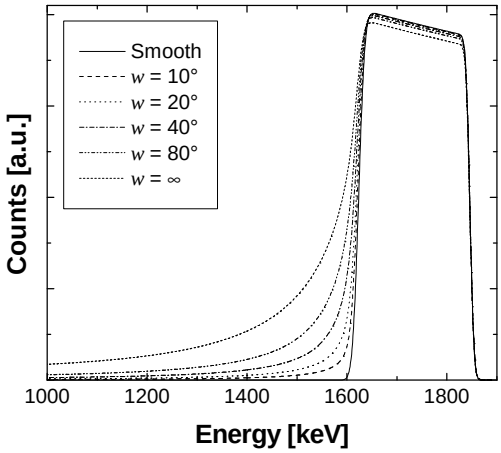

Fig. 7. Calculated energy spectra for 2 MeV ^{4}He backscattered from a gold layer with thickness 1×10^{18} Au-atoms/cm^2 on a rough substrate with different roughnesses. The roughness is described by a Lorentz distribution of tilt angles with FWHM w. $w = \infty$ is an equipartition of tilt angles. Incident angle $\alpha = 0°$, scattering angle 165°.

layer thickness was about 3.5 μm, while the standard deviation of the substrate roughness, as determined with a profiler at different areas and different scan directions parallel and perpendicular to the carbon fibres, was about 8.2 μm, i.e. the substrate roughness was considerably larger than the thickness of the W layer. The measured tilt angle distribution could be fitted reasonably well with a Lorentz distribution having a FWHM of 26.6°. The amounts of impurities in the W layer were determined by X-ray fluorescence analysis (Ni, Fe, Cr) and secondary ion mass spectrometry (SIMS) (C, O). The impurity concentration was < 2 at.% and does not contribute significantly to the measured spectrum. Impurities were neglected in the simulations.

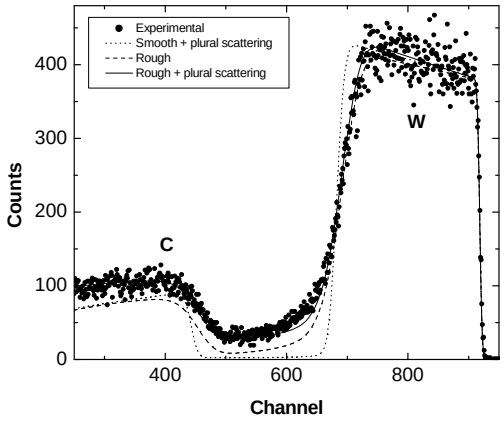

Fig. 8. 2.5 MeV protons backscattered from 3.5 μm W on a rough carbon substrate, normal incidence, scattering angle 165°. Dots: Experimental data; Dotted line: Calculated spectrum for a smooth W layer (3.6 μm) on a smooth C substrate including plural scattering; Dashed line: Calculated spectrum for a rough W layer (3.5 μm, $\sigma = 0.30\,\mu$m) on a rough substrate (FWHM 20°); Solid line: As dashed line, but including plural scattering.

The dotted line in Fig. 8 is the calculated spectrum for a smooth W layer on a smooth carbon substrate. Plural scattering in the W layer was included in dual scattering approximation [26]: All trajectories with two scattering events in the W layer are taken into account. Plural scattering results in the small background visible between the carbon and tungsten signals in channels 500–650. This spectrum has only minor resemblance with the experimental curve, and requires a slightly thicker W layer (3.6 μm) for best fit. The dashed line is calculated for a rough W layer, characterized by a Gamma-distribution of layer thicknesses with a mean thickness of 3.5 μm and standard deviation $\sigma = 0.3\,\mu$m on a rough carbon substrate, characterized by a Lorentz distribution of tilt angles with FWHM = 20°. The roughnesses of the layer and the substrate are assumed to be independent, and plural scattering is not taken into account. The W peak (channels > 650) is already well described, but the low energy tail below the peak is underestimated. The solid line uses the same roughness parameters for the W-layer and the substrate, but takes additionally plural scattering in the W-layer into account. Now the whole experimental spectrum is reproduced well, with only a small discrepancy in channels 600–650. Compared to the smooth layer the contribution of plural scattering has increased strongly, which is due to an enhancement of plural scattering at oblique incidence. The height and shape of the low energy tail below the W-peak in channels < 650 are determined by the wings of the tilt angle distribution with inclination angles $> \pm 45°$. The measured tilt angle distribution could be described by a Lorentz distribution with a FWHM of 26.6°, while the best fit to the measured spectrum yields a FWHM of about 20°. Inaccuracies in the measurement of the tilt angle distribution at high inclinations due to the apex angle of the profiler tip and the constant step width, together with uncertainties in the calculation of the plural scattering background, are the reason for this small discrepancy. Additionally it should be kept in mind that the used model of inclined line segments, see Fig. 1, is only an approximation to physical reality, and the real surface has an additional fine structure, which is often described by fractal geometry [32,33].

The influence of the different roughnesses on the shape of the RBS spectrum is shown in more detail in Fig. 9. The experimental data (black dots) and the solid line in the top and bottom figures are the same as in Fig. 8. The substrate roughness is kept constant in Fig. 9 (top), and the roughness of the W layer is varied from smooth to 0.6 μm. The roughness of the W-layer influences mainly the low energy edge of the W peak, best fit is obtained for $\sigma = 0.3$ μm. The bottom part shows the influence of the carbon substrate roughness for constant W-layer roughness. Substrate roughness influences mainly the low energy tail below the W-peak, while the low energy edge of the W-peak is less affected by substrate roughness. Best fit is obtained for about 20° FWHM. Due to the different effects of the two roughnesses on the shape of RBS spectra the two roughnesses can be easily distinguished.

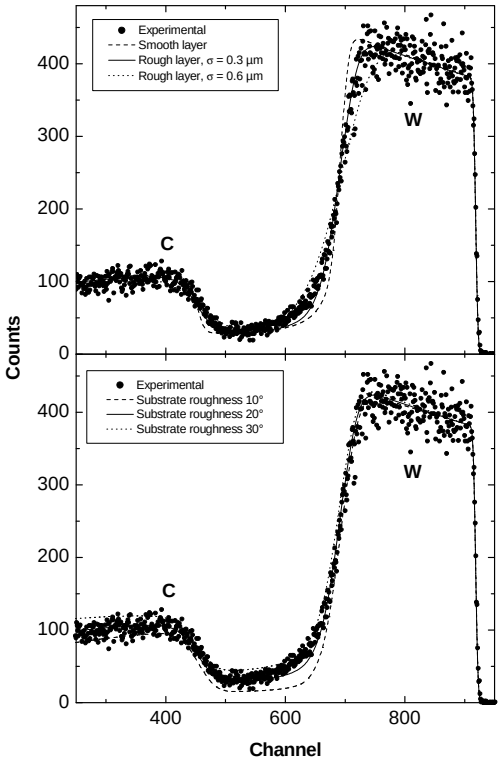

Fig. 9. Same experimental data as in Fig. 8, compared to simulation calculations with different roughness parameters. Top: Calculations for a rough carbon substrate (FWHM 20°) and different W-layer roughnesses, characterized by a Gamma-distribution with standard deviation σ; Bottom: Calculations for a rough W layer ($\sigma = 0.3$ μm) and different substrate roughnesses, characterized by a Lorentz-distribution of tilt angles with different FWHM's. Mean W-layer thickness 3.5 μm, plural scattering included.

6 Conclusions

The influence of surface roughness on RBS spectra has been studied experimentally and by computer simulations with the SIMNRA code, versions 4.70 and higher. The program can calculate the effects of film roughness, substrate roughness, and combinations of both. Rough films are described by a Gamma distribution of film thicknesses, while rough substrates are approximated by a Lorentz distribution of local inclination angles. Correlation effects of film roughness, such as incidence through a valley and emergence through a hump or multiple surface crossings, are neglected. This approximation is well fulfilled for typical RBS geometries at backscattering angles in the range 150–180° and non-grazing incidence and emergence angles, but may be less valid for typical ERDA geometries at grazing incidence and exit angles.

The computing time increases from about 1 s for a simple RBS-spectrum of a smooth layer to about 10–30 s for a rough layer on a 500 MHz Pentium 3 processor. Film roughness can be used for evaluation of RBS including non-Rutherford scattering, NRA and ERDA.

In RBS geometry, layer roughness results in a smearing of the low energy edge of thin films and the development of tails stretching to low energies. The shape of this smearing is different for film and substrate roughness due to the different distribution functions. For rough films the energy at which the low energy edge has decreased to its half value is a rather robust measure of the mean film thickness, as long as the width of the thickness distribution is lower than its mean thickness. This is not the case for substrate roughness. Additionally plural scattering may play an important role on rough substrates, if the films contain high-Z elements.

Results of simulation calculations are in good agreement with experimental data and measured surface roughnesses. The ability to calculate surface roughness effects enables quantitative ion beam analysis of thin films even under extreme conditions, such as films with roughness exceeding the mean film thickness or films on very rough substrates like carbon fibre composites or plasma sprayed materials.

Acknowledgements

Helpful discussions with R. Fischer and Prof. V. Dose about distribution functions are gratefully acknowledged. The W-layers on CFC were measured by T. Dittmar, Garching.

References

[1] J.R. Tesmer and M. Nastasi, Eds. *Handbook of Modern Ion Beam Materials Analysis*. Materials Research Society, Pittsburgh, Pennsylvania, 1995.

[2] R. Doolittle. Nucl. Instr. Meth. B9 (1985) 344.

[3] R. Doolittle. Nucl. Instr. Meth. B15 (1986) 227.

[4] M. Mayer. SIMNRA user's guide. Tech. Rep. IPP 9/113, Max-Planck-Institut für Plasmaphysik, Garching, 1997.

[5] M. Mayer. SIMNRA, a simulation program for the analysis of NRA, RBS and ERDA. In *Proceedings of the 15th International Conference on the Application of Accelerators in Research and Industry* (1999), J. L. Duggan and I. Morgan, Eds., vol. 475 of *AIP Conference Proceedings*, American Institute of Physics, p. 541.

[6] R.D. Edge and U. Bill. Nucl. Instr. Meth. 168 (1980) 157.

[7] A.R. Knudson. Nucl. Instr. Meth. 168 (1980) 163.

[8] J.R. Bird, P. Duerden, D.D. Cohen, G.B. Smith, and P. Hillery. Nucl. Instr. Meth. 218 (1983) 53.

[9] C.P. Hobbs, J.W. McMillan, and D.W. Palmer. Nucl. Instr. Meth. B30 (1988) 342.

[10] M. Wüest and P. Bochsler. Nucl. Instr. Meth. B71 (1992) 314.

[11] I.M. Yesil. Einfluß der Oberflächenrauhigkeit auf ERDA-Tiefen-Profile. Master's thesis, Ludwig Maximilian Universität, München, 1995. In german.

[12] I.M. Yesil, W. Assmann, H. Huber, and K.E.G. Löbner. Nucl. Instr. Meth. B136-138 (1998) 623.

[13] A. Kitamura, T. Tamai, A. Taniike, Y. Furuyama, T. Maeda, N. Ogiwara, and M. Saidoh. Nucl. Instr. Meth. B134 (1998) 98.

[14] R. Behrisch, S. Grigull, U. Kreissig, and R. Grötschel. Nucl. Instr. Meth. B136-138 (1998) 628.

[15] V.S. Shorin and A.N. Sosnin. Nucl. Instr. Meth. B72 (1992) 452.

[16] H. Metzner, M. Gossla, and Th. Hahn. Nucl. Instr. Meth. B124 (1997) 567.

[17] H. Metzner, Th. Hahn, M. Gossla, J. Conrad, and J.-H. Bremer. Nucl. Instr. Meth. B134 (1998) 249.

[18] H.H. Andersen and J.F. Ziegler. *Hydrogen - Stopping Powers and Ranges in All Elements*, vol. 3 of *The Stopping and Ranges of Ions in Matter*. Pergamon Press, New York, 1977.

[19] J.F. Ziegler. *Helium - Stopping Powers and Ranges in All Elements*, vol. 4 of *The Stopping and Ranges of Ions in Matter*. Pergamon Press, New York, 1977.

[20] J.F. Ziegler, J.P. Biersack, and U. Littmark. *The Stopping and Range of Ions in Solids*, vol. 1 of *The Stopping and Ranges of Ions in Matter*. Pergamon Press, New York, 1985.

[21] J.F. Ziegler and J.M. Manoyan. Nucl. Instr. Meth. B35 (1988) 215.

[22] W.K. Chu. Phys. Rev. 13 (1976) 2057.

[23] J.W. Mayer and E. Rimini. *Ion Handbook for Material Analysis*. Academic Press, New York, San Francisco, London, 1977.

[24] E. Szilágy, F. Pászti, and G. Amsel. Nucl. Instr. Meth. B100 (1995) 103.

[25] E. Szilágy. Nucl. Instr. Meth. B161-163 (2000) 37.

[26] W. Eckstein and M. Mayer. Nucl. Instr. Meth. B153 (1999) 337.

[27] M. Mayer, R. Behrisch, C. Gowers, P. Andrew, and A.T. Peacock. Change of the optical reflectivity of mirror surfaces exposed to JET plasmas. In *Diagnostics for Experimental Thermonuclear Fusion Reactors 2*, P. Stott, G. Gorini, P. Prandoni, and E. Sindoni, Eds. Plenum Press, New York, London, 1998, p. 279.

[28] M. Mayer, R. Behrisch, P. Andrew, and A.T. Peacock. J. Nucl. Mater. 241-243 (1997) 469.

[29] M. Küstner, W. Eckstein, E. Hechtl, and J. Roth. J. Nucl. Mater. 265 (1999) 22.

[30] R. Fischer and M. Mayer. to be published.

[31] R. Amirikas, D.N. Jamieson, and S.P. Dooley. Nucl. Instr. Meth. B77 (1993) 110.

[32] D. Avnir, D. Farin, and P. Pfeifer. Nature 308 (1984) 261.

[33] M. Mayer, W. Eckstein, and B.M.U. Scherzer. J. Appl. Phys. 77, 12 (1995) 6609.